ORIGINAL ARTICLE

Effects of lap configuration on mechanical properties and composition distribution of three-layer overlapped laser weldments on Al/Cu dissimilar materials

Joonghyeon Shin[1] · Minjung Kang[1]

Abstract

Battery cells are connected via bus-bars to meet performance requirements, such as power and capacity, and multiple layers of dissimilar materials functioning as anodes, cathodes, or bus-bars are overlapped and welded together. In laser welding, the formation of brittle intermetallic phases in the weld joint is inevitable and, in turn, deteriorates the mechanical properties. To obtain the desirable joint performance, appropriate welding parameters to avoid intermetallic phase formations and joint designs to release stress concentrations must be obtained. This study investigates the effects of lap configurations and process parameters on the tensile-shear load, T-peel load, and composition distribution when multi-layered joints of dissimilar materials are produced by laser welding. Two layers of 0.4 mm Al sheets were welded with a single 0.2 mm Cu sheet, which was emulated using electric vehicle battery interconnects. The results show that the penetration depth varied in accordance with the lap configuration even under the same heat input condition. The lap configuration and welding parameters influenced the composition distribution of the welds, as they altered the solidification rate, number of Cu/Al contact interfaces, and location of the high-density material. The failure load of the T-peel specimens was lower than that of the tensile-shear specimens except for the Cu − Al − Al lap configuration. The T-peel load of the Cu − Al − Al lap configuration was similar to that of the tensile-shear load. When the stress-concentrated joint was homogeneous, it was more robust.

Keywords Al/Cu dissimilar welding · Single-mode laser welding · Three-layer overlap welding · Tensile-shear strength · T-peel strength · Component distribution

1 Introduction

Al and Cu are often inevitable in microelectronics and alternative energy devices, as well as in secondary batteries for hybrid vehicles and fuel cells [1, 2]. In the battery assembly, a large number of battery cells are connected via bus-bars to meet performance requirements, such as power and capacity [3]. In such stacking configurations, multiple layers of dissimilar materials, mostly copper, nickel, or aluminum, are welded together and function either as anodes, cathodes, or bus-bars [4, 5]. Achieving consistent weld qualities and properties in the multiple-weld interfaces is critical for reliable battery assembling and electric vehicle performance [6].

However, joining dissimilar materials is challenging due to the differences in their chemical, physical, and thermal properties, such as melting temperatures, thermal diffusivities, and thermal expansion/shrinkage [6–8]. In addition, brittle intermetallic phase (IMP) formations [7] due to the chemical reaction between Al and Cu is inevitable, causing a decrease in the bonding strength and a low electrical conductivity [7, 9]. The existence of thick IMPs at the joining interface causes the appearance of numerous cracks and pores [6, 10–12]. Braunovic et al. [13] reported that the deleterious effect of IMPs is reflected in the brittleness of the joint, and a higher contact resistance results based on the thickness of the IMPs formed. Lee et al. [14] reported that strong laser-welded joints could be produced at high welding speeds by suppressing the formation of intermetallic phases.

Various joining techniques involving the use of lasers [14–16], friction stir [17, 18], diffusion [19], and ultrasonic welding

✉ Minjung Kang
  kmj1415@kitech.re.kr

[1] Advanced Joining and Additive Manufacturing R&D Department, Korea Institute of Industrial Technology, Incheon, Republic of Korea

[20–23] have been employed in the fabrication of Al−Cu dissimilar joints. In fusion welding, such as laser welding, severe IMPs can be easily formed by the melting of the material compared to other solid-state welding processes such as ultrasonic welding. Nevertheless, the laser welding technology in energy device manufacturing is expected to improve the joint quality and production efficiency by alternating between ultrasonic processes based on the advantages of high precision, high flexibility, and repeatability [24]. Studies on achieving multiple layers of Al−Cu joints using laser welding (or fusion welding) have not yet been reported. However, extensive studies have been conducted on laser-welded specimens using two material sheets. Consequently, a better understanding of the joint formation in multilayered laser-welded Al and Cu dissimilar joints is highly desired to obtain process productivities with sound joint qualities.

Minimization of IMPs can be accomplished by suppressing the intermixture of metals and reducing the processing time to avoid diffusion. Huang et al. [25] demonstrated the concentration behavior of Cu in a Cu (top)−Al (bottom) dissimilar material joint via a multi-physics numerical model and ex situ element mapping. They proved that the concentration of Cu in the top region of the molten pool was over 50 wt% under high-speed welding conditions as a result of the upward flow in the molten pool that is driven by the recoil pressure. The element mixing process in laser keyhole welding is affected by the laser power, welding speed, and heat input [25]. This indicates that proper welding parameters are required to suppress the formation of IMPs to obtain desirable joint characteristics, such as ductility and toughness.

This study investigates the effects of process parameters on the mechanical properties and composition distribution when multilayered joints of dissimilar materials are produced by laser welding. Two layers of 0.4 mm Al sheets were welded with a single 0.2 mm Cu sheet that was emulated by electric vehicle battery interconnects. Joint robustness was assessed by performing tensile-shear and T-peel tests on the specimens fabricated under various welding speed conditions. The present study attempted to evaluate the effect of lap configurations on the composition distribution and hardness and their relationships with the tensile-shear and T-peel loads.

2 Experimental setup

A single-mode fiber laser (CFL-1000, Nlight, USA) was used for welding. The beam was delivered through an optical fiber with a diameter of 14 μm and a two-axis scanner system (hurrySCAN30, Scanlab, Germany) with a focal length of 405.5 mm. The beam was irradiated perpendicularly onto the specimen placed at the focal position. At the focal point, the laser beam had a beam diameter of 35.7 μm.

The base materials were nickel-coated C1020 (thickness: 0.2 mm) and Al1050 (thickness: 0.4 mm). The mechanical

Table 1 Mechanical properties and chemical composition of used materials (as-received)

	Mechanical properties (MPa, %)		
	Tensile strength	Yield strength	El
C1020	250	210	33.0
Al1050	110	94	8.4
	Chemical composition (wt.%)		
	Cu	Al	Mg
C1020	> 99.95	-	-
Al1050	0.05	> 99.5	0.4

properties and chemical composition of used materials are presented in Table 1. The thickness of coated material on copper was approximately 2 μm. The specimen was prepared with a width of 40 mm and length of 45 mm. Figure 1 shows the detailed geometry of the welding joint configuration for the tensile-shear and T-peel test specimens. The gap between the layers was set to 0 mm, and the overlap length was 10 mm. During the welding, the specimens were fixed with a spring-type high-precision jig to maintain a zero-gap between the sheets. Laser overlap welding was performed with a length of 40 mm at the center of
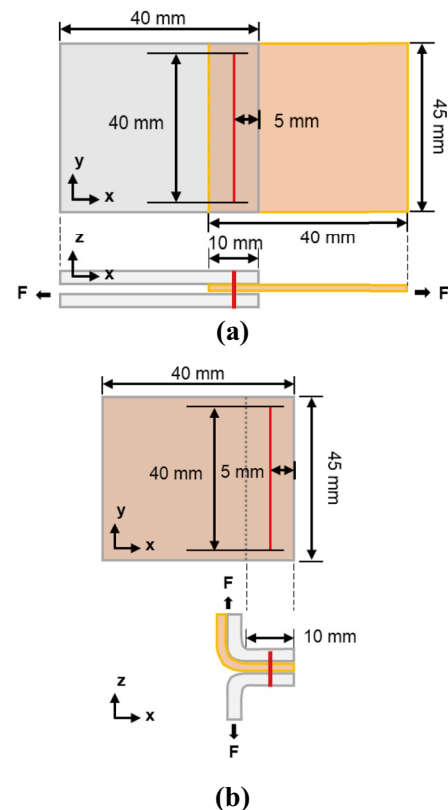

Fig. 1 Schematic diagram of **a** tensile-shear and **b** T-peel specimens of ACA lap configuration

overlapped width, that is, at a distance of 5 mm away from the edge. During the welding, shielding gases were not provided.

The laser power was maintained at 1 kW, and the welding speed was varied from 250 to 450 mm/s to obtain various heat input conditions. In addition, Al−Al−Cu (AAC), Al−Cu−Al (ACA), and Cu−Al−Al (CAA) three-layer lap configurations were selected to evaluate the effect of the stacking sequence on the mechanical properties and component distributions.

Tensile-shear and T-peel tests were performed on the welded length of 40 mm, including the start and end points, to imitate the battery interconnection assembly. The joint failure load was evaluated at the interface between the second and third layers, which is a relatively narrow and weak interface due to the consumption of energy [22]. Each tensile-shear and T-peel test specimens were tested three times, and the average value was calculated.

The transverse cross sections were polished and observed using optical microscopy and field-emission scanning electron microscopy (FE-SEM). The micro-Vickers hardness of the cross section was measured with an indent spacing of 0.1 mm along the centerline of the welds. The applied load and holding time for the hardness measurements were 490 N and 10 s, respectively. The chemical composition of the macro-sections was analyzed via energy-dispersive X-ray spectroscopy to confirm the formation of intermetallic phases.

3 Results and discussion

3.1 Effect of lap configuration on penetration depth

The penetration depth was varied depending on the lap configuration under the same heat input conditions, as depicted in Fig. 2. As the welding speed increased, the heat input decreased, and the penetration depth tended to be shallow. At a welding speed of 350 mm/s, the penetration depth converted from full penetration to partial penetration. The reductions in penetration depth for the CAA and ACA lap configurations were greater than that for the AAC configuration. This is because when the Cu layer was placed closer to the focused laser beam, the heat input quickly dissipated to the surroundings [25], due to the high melting point and thermal diffusivity of copper. Another reason for this difference was the fact that lasers with wavelengths greater than 1 μm exhibit a low absorption rate for copper [26].

The melted zone of the Cu layer was narrower than that of the Al layer due to its thermal properties, as shown in Fig. 3. All specimens had sound weld cross sections without cracks, except under over-welded conditions. Some pores were formed near the fusion line of the Al layer as indicated by arrows in Fig. 3. This can be explained by the turbulent melt-pool dynamics that have been reported by other researchers [12, 15].
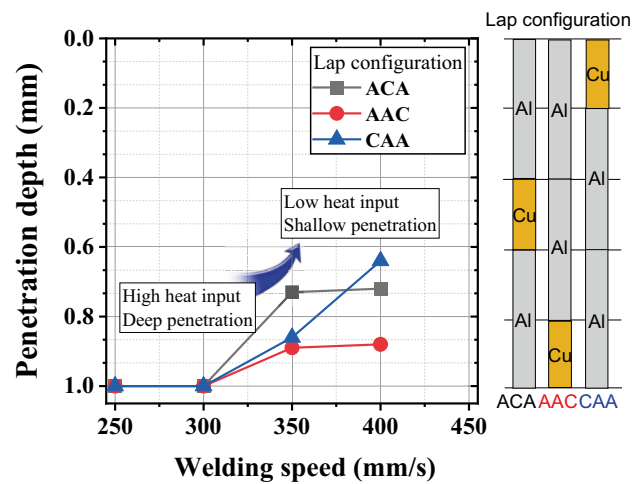

Fig. 2 Penetration depth measurement according to the lap configuration and welding speed

3.2 Effect of lap configuration on composition distribution

The chemical composition distribution of the weld was affected by the lap configuration and the welding parameters. The recoil pressure induced by the laser keyhole movement stirred the molten pool, thus resulting in the mixing of components in
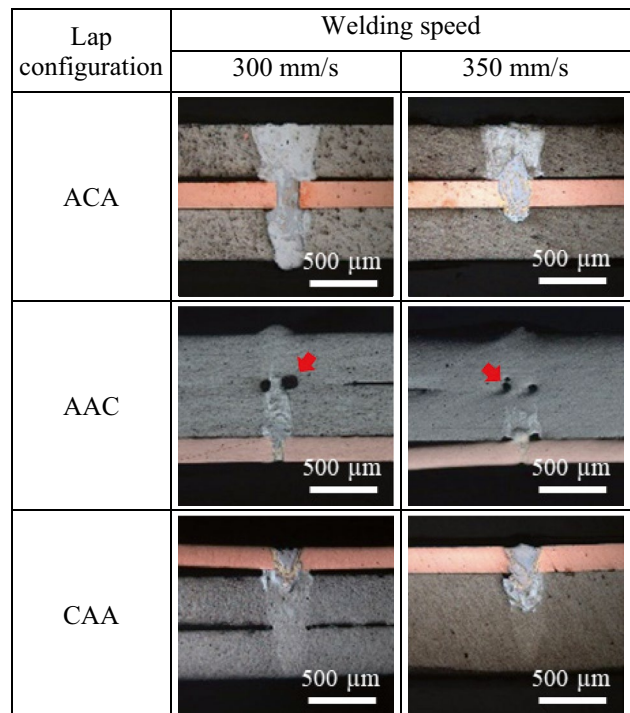

Fig. 3 Macro-sectional images according to the lap configuration and welding speed
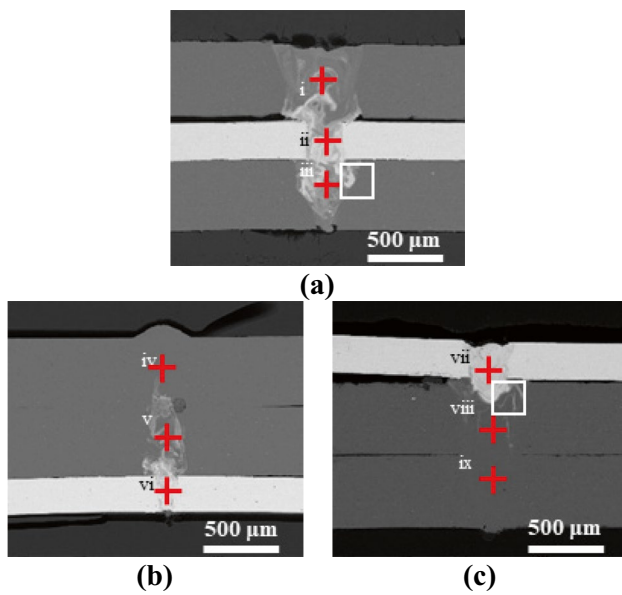
Fig. 4 FE-SEM images of overlapped joint with various lap configurations under a welding speed of 300 mm/s; **a** ACA; **b** AAC; **c** CAA

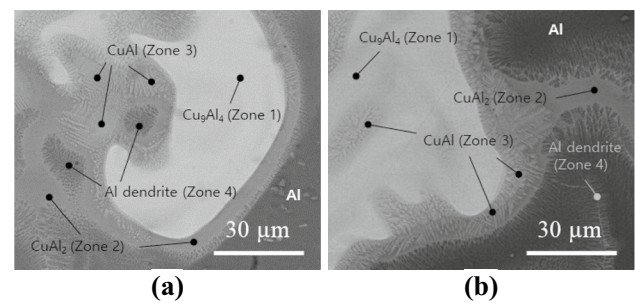**Fig. 5** SEM images of the fusion zone for **a** ACA and **b** AAC lap configurations, indicated by white boxes in Fig. 4

each layer. However, Al and Cu are not entirely mixed throughout the molten pool. Huang et al. [25] demonstrated no homogeneous element distribution in the weld metal via the finite element model and EDS element mapping. Li et al. [27] investigated the relationship between the laser welding speed and element concentration and revealed that fast welding speed deteriorated uniform element distribution due to insufficient reaction time. They noted that surface tension and viscosity during mass transfer also affect the constitution of weld metal.

Compositional analysis was performed on the cross section of the welds in the middle of each layer, and the results are presented in Fig. 4 and Table 2. In the specimens with the ACA lap configuration, the Cu component was distributed throughout

the fusion zone regardless of the welding speed, while for the AAC and CAA lap configuration specimens, the Cu component was concentrated near the Cu layer. For the ACA lap configuration, the Cu content reached 69.7% at a welding speed of 300 mm/s, whereas 92.3% and 83.8% of Cu content were measured in the AAC and CAA lap configurations, respectively. The dilution behavior and distribution of constitutional elements were altered depending on the location of the high-density Cu layer. The elements were blended in a relatively narrow region when the welding speed was increased to 350 mm/s (Fig. 3). It can be predicted that the composition distribution was restricted with increasing welding speed due to the fast solidification rate.

From these results, it can be concluded that the distribution of the composition within the weld was affected by the lap configuration and welding speed. The number of Cu/Al contact interfaces (diffusion paths), the different behavior of the molten pool induced by the difference in density of each composition [14], and the solidification rate acted in a complicated manner inside the welds.

During the solidification process, a solution is formed via the stirring and diffusion of Al and Cu in the liquid state. The Cu content in the composition gradually decreased from the Cu-rich side to the Al-rich side, independent of the lap configuration. Measured chemical composition of IMPs (Table 3) was in good agreement with the results of other literatures as shown in Table 4. The IMPs of Al/Cu were divided into four zones, which could be distinguished by their morphology and chemical compositions; Zone 1 consisted of γ-Cu_9Al4 in the form of columnar grains. Zone 2 was a mixture of lumpish

Table 2 Measured chemical composition used EDX. The measured locations are marked in Fig. 5

Lap configuration	Measuring position	Chemical composition (wt%)	
		Al	Cu
ACA	i	30.3	69.7
	ii	32.4	67.6
	iii	34.2	65.8
AAC	iv	92.8	7.8
	v	83.0	17.0
	vi	6.7	92.3
CAA	vii	16.2	83.8
	viii	19.3	80.7
	ix	100	0

Table 3 EDX analytical results of weld metal; zone 1 to zone 4

Zone	Chemical composition (at%)		Possible phase
	Al	Cu	
1	62–69	31–38	Cu_9Al_4
2	28–35	64–72	$CuAl_2$
3	44–46	54–55	CuAl
4	7–14	86–92	Al

Table 4 IMPs in the Al-Cu system depending on process

Phase	Nominal composition	% et al	Hardness (HV)	Processes						
				Bimetal casting	Laser brazing	Diffusion bonding	Electron beam welding*	Laser welding	Laser welding	Laser welding
Cu		0–19.7								
γ	Al$_4$Cu$_9$	31–37.5	750–770	-	found	-	found	found	found	-
ζ	Al$_3$Cu$_4$	43.7–44.8	624–930	-	found	-	-	-	-	-
η	AlCu	47.6–50.2	648–905	found	found	found	-	found	found	found
θ	Al$_2$Cu	67–68.1	413–650	found	found	found	found	found	found	found
Al		98.52–100								
Reference				Travassoli, 2016 [28]	Schmalen, 2016 [7]	Xiong, 2018 [11]	Otten, 2016 [29]	Zuo, 2014 [6]	Lee, 2014 [14]	Yan, 2019 [30]

*Note) 3rd phase found

and net-like eutectic and hypoeutectic structures of α-Al and θ-CuAl$_2$. Zone 3 consisted of a fine eutectic structure with α-Al and θ phases. Zone 4 consisted of an α-Al dendritic structure near the Al layer. In this study, the shape and arrangement of zones were randomly formed because the laser welding speed was extremely fast and thus resulted in solute trapping during the rapid solidification process, as shown in Fig. 5.

3.3 Effect of lap configuration on mechanical characteristics

Higher hardness values were measured in the fusion zone than in the base materials due to the chemical reaction between Al and Cu. The hardness of the base materials Cu and Al was 87.5 HV and 47.6 HV, respectively, while the hardness of the welds was in the range of 45 − 649 HV. As shown in Fig. 6, a rapid change in the hardness was observed near the Al − Cu
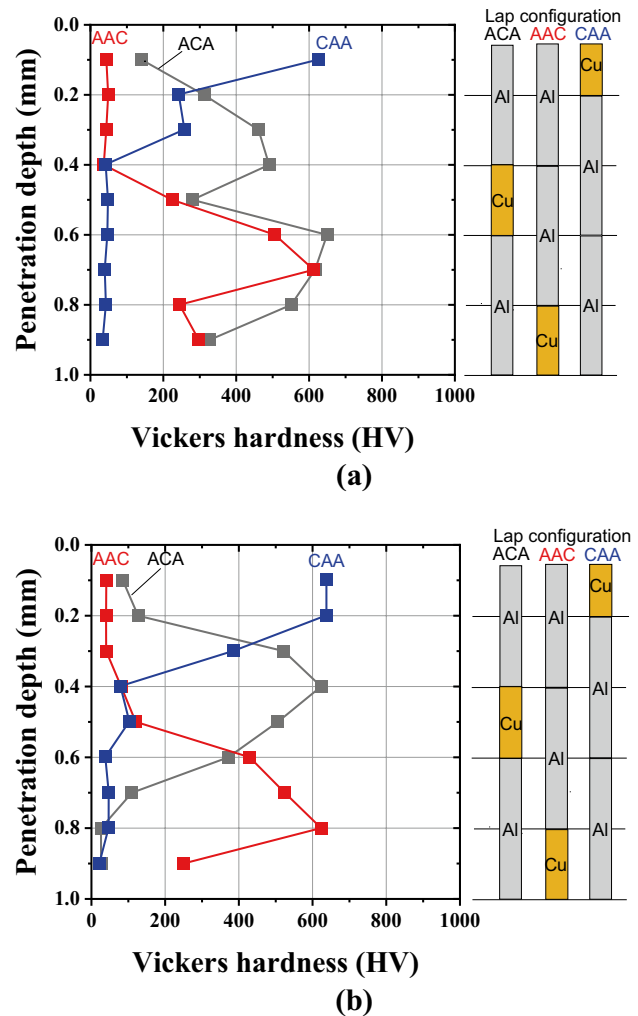
(a)

(b)

Fig. 6 Hardness profile according to the lap configuration. The specimens were fabricated with welding speed of **a** 300 and **b** 350 mm/s

interface, where intermetallic phases could be generated. The formation of intermetallic phases in the welds is promoted when a high heat input is applied to the specimen. The Cu diffusion distance of AAC was shorter than that of the other lap configurations because the diffusion path was only allowed to a faying interface. Thus, it can be concluded that the lap configuration affected the hardness distribution of the welds.

The tensile-shear load also differed depending on the lap configuration and welding parameters (Fig. 7a). The tensile-shear loads tended to decrease in the AAC and CAA lap configurations as the interface width narrowed with an increase in the welding speed. However, in the ACA lap configuration, the tensile-shear strength increased up to a welding speed of 350 mm/s and then decreased. In general, the load carrying capacity is positively related to the size of welds and heat input. However, the formation of IMPs was accelerated and
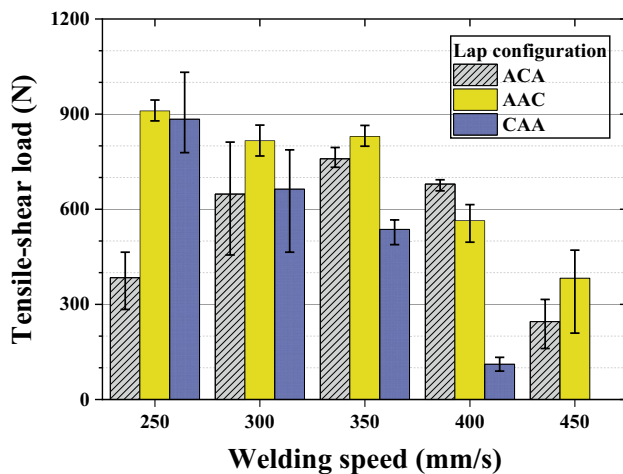
(a)
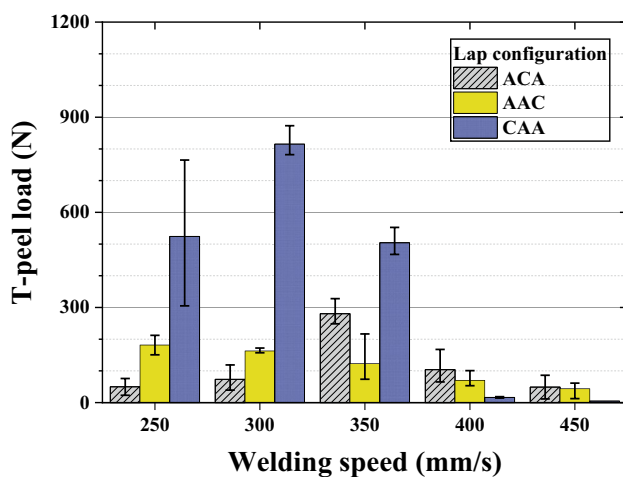
(b)

Fig. 7 Measured tensile-shear and T-peel load depending on the lap configuration
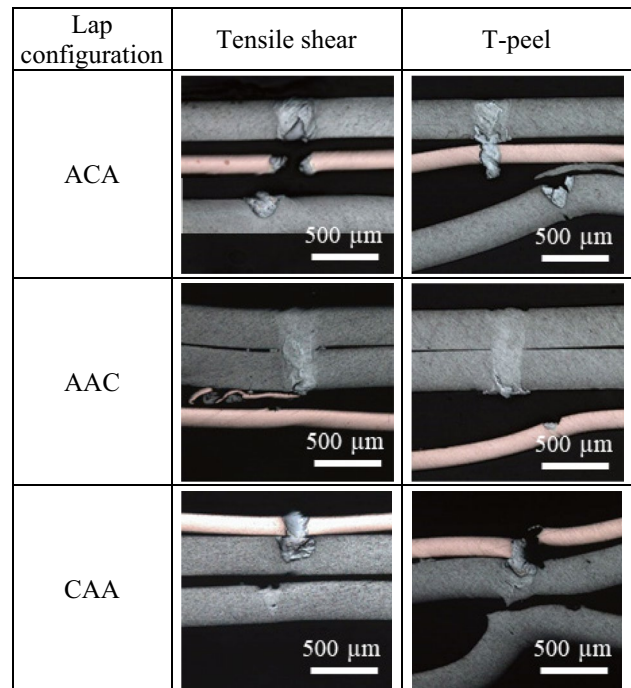

Fig. 8 Macro-sectional images after tensile-shear and T-peel tests with differential lap configuration. The specimens were manufactured at a welding speed of 350 mm/s

joint properties deteriorated with the increase in heat input. As a result of the tensile-shear test, an interfacial rupture occurred in all fabricated specimens regardless of the lap configuration (Fig. 8).

The failure loads of the T-peel test were lower than those of the tensile-shear loads in present study (Fig. 7b). When the welding speed was 250–350 mm/s, the failure load with the CAA lap configuration was evaluated to be higher than that of the AAC or ACA lap configurations. In the CAA case, the hardness values at the interfacial joint between the second and third layers were maintained at a low value, as shown in the hardness profile (Fig. 6). Thus, it can be inferred that the failure was not affected by the formation of brittle IMPs in the CAA case. If the materials were consistent at the interface, the joint would have been more robust because the force was transferred by detouring the IMPs. Interfacial and pull-out mode fractures were also observed (Fig. 8).

4 Conclusion

This study investigated joint formation in multilayered laser welding subject to various process parameters. The results are as follows:

1. The penetration depth varied according to the lap configuration even under the same heat input condition due to the different laser power deliveries results from different beam absorption rates of Al and Cu. In addition, the high heat capacity and thermal diffusivity of copper allowed the transferred energy to be easily dissipated to the surroundings.

2. The chemical composition distribution of the weld was affected by the lap configuration and the welding parameters. The forces induced by the recoil pressure are limited to stirring the molten pool, resulting in a non-uniform distribution of the layer components. The element distribution appears to be affected by the solidification rate, the number of Cu/Al contact interfaces, and the position of the high-density material.

3. The tensile-shear and T-peel loads were affected by the lap configurations and welding parameters. The failure load of the T-peel specimens was lower than that of the tensile-shear specimens. Thus, designing joints to avoid stress concentration and the formation of brittle IMPs is essential to obtain desirable joint performance.

Author contribution Joonghyeon Shin contributed to conceptualization, methodology, writing. Minjung Kang helped in supervision review, data curation and editing, funding acquisition.

Data availability No additional data available.

Code availability Not applicable.

Declarations

Ethical approval No ethical approval was required for this research.

Consent to participate Not applicable.

Consent to publish All authors have read and agreed to the published version of the manuscript.

Competing interests The authors declare no competing interests.

References

1. Chu S, Majumdar A (2012) Opportunities and challenges for a sustainable energy future. Nature 488(294):1–13. https://doi.org/10.1038/nature11475
2. Das A, Li D, Williams D, Greenwood D (2018) Joining technologies for automotive battery systems manufacturing. World Electr Veh J 9(22):1–13. https://doi.org/10.3390/wevj9020022
3. Lee SS, Kim TH, Hu SJ, Cai WW, Abell JA (2015) Analysis of weld formation in multilayer ultrasonic metal welding using high-speed images. J Manuf Sci Eng 137(3): 031016–1–8. https://doi.org/10.1115/1.4029787
4. Lee WB, Bang KS, Jung SB (2005) Effects of intermetallic compound on the electrical and mechanical properties of friction welded Cu/Al bimetallic joints during annealing. J Alloys Compd 390:212–219. https://doi.org/10.1016/j.jallcom.2004.07.057
5. Solchenbach T, Plapper P (2013) Mechanical characteristics of laser braze-welded aluminium–copper connections. Opt Laser Technol 54:249–256. https://doi.org/10.1016/j.optlastec.2013.06.003
6. Zuo D, Hu S, Shen J, Xue Z (2014) Intermediate layer characterization and fracture behavior of laser-welded copper/aluminum metal joints. Mater Des 58:357–362. https://doi.org/10.1016/j.matdes.2014.02.004
7. Schmalen P, Plapper P (2016) Evaluation of laser braze-welded dissimilar Al–Cu ioints. Phys Procedia 83:506–514. https://doi.org/10.1016/j.phpro.2016.08.052
8. Xue Z, Hu S, Zuo D, Cai W, Lee D, Elijah KA (2013) Molten pool characterization of laser lap welded copper and aluminum. J Phys D Appl Phys 46:495501-1–495509. https://doi.org/10.1088/0022-3727/46/49/495501
9. Schmalen P, Plapper P, Cai W (2016) Process robustness of laser braze-welded Al/Cu connectors. SAE Int J Altern Powertrains 5(1):195–204. https://doi.org/10.4271/2016-01-1198
10. Zhou L, Li Z, Song X, Tan C, He Z, Huang Y, Feng J (2017) Influence of laser offset on laser welding-brazing of Al/brass dissimilar alloys. J Alloys Compd 717:78–92. https://doi.org/10.1016/j.jallcom.2017.05.099
11. Xiong J, Peng Y, Zhang H, Li J, Zhang F (2018) Microstructure and mechanical properties of Al-Cu joints diffusion-bonded with Ni or Ag interlayer. Vacuum 147:187–193. https://doi.org/10.1016/j.vacuum.2017.10.033
12. Solchenbach T, Plapper P, Cai W (2014) Electrical performance of laser braze-welded aluminum–copper interconnects. J Manuf Processes 16:183–189. https://doi.org/10.1016/j.jmapro.2013.12.002
13. Braunovic M (2017) Reliability of power connections. J Zhejiang Univ Sci A 8(3):343–356. https://doi.org/10.1631/jzus.2007.A0343
14. Lee SJ, Nakamura H, Kawahito Y, Katayama S (2014) Effect of welding speed on microstructural and mechanical properties of laser lap weld joints in dissimilar Al and Cu sheets. Sci Technol Weld Joining 19(2):111–118. https://doi.org/10.1179/1362171813Y.0000000168
15. Kraetzsch M, Standfuss J, Klotzbach A, Kaspar J, Brenner B, Beyer E (2011) Laser beam welding with high-frequency beam oscillation: Welding of dissimilar materials with brilliant fiber lasers. Phy Procedia 12:142–149. https://doi.org/10.2351/1.5062231
16. Mai T, Spowage A (2004) Characterisation of dissimilar joints in laser welding of steel–kovar, copper–steel and copper–aluminium. Mater Sci Eng A 374:224–233. https://doi.org/10.1016/j.msea.2004.02.025
17. Tan C, Jiang Z, Li L, Chen Y, Chen X (2013) Microstructural evolution and mechanical properties of dissimilar Al–Cu joints produced by friction stir welding. Mater Des 51:466–473. https://doi.org/10.1016/j.matdes.2013.04.056
18. Sahin M (2010) Joining of aluminium and copper materials with friction welding. Int J Adv Manuf Technol 49:527–534. https://doi.org/10.1007/s00170-009-2443-7
19. Abbasi M, Taheri AK, Salehi M (2001) Growth rate of intermetallic compounds in Al/Cu bimetal produced by cold roll welding process. J Alloys Compd 319:233–241. https://doi.org/10.1016/S0925-8388(01)00872-6
20. Satpathy MP, Sahoo SK (2017) Mechanical performance and metallurgical characterization of ultrasonically welded dissimilar joints. J Manuf Processes 25:443–451. https://doi.org/10.1016/j.jmapro.2017.01.001

21. Xi L, Banu M, Hu SJ, Cai W, Abell J (2017) Performance prediction for ultrasonically welded dissimilar materials joints. J Manuf Sci Eng 139(1): 011008–1–13. https://doi.org/10.1115/1.4033692

22. Das A, Masters I, Williams D (2019) Process robustness and strength analysis of multi-layered dissimilar joints using ultrasonic metal welding. Int J Adv Manuf Technol 101:881–900. https://doi.org/10.1007/s00170-018-2936-3

23. Luo Y, Chung H, Cai W, Rinker T, Hu SJ, Kannatey-Asibu E, Abell J (2018) Joint formation in multilayered ultrasonic welding of Ni-coated Cu and the effect of preheating. J Manuf Sci Eng 140(11): 111003–1–10. https://doi.org/10.1115/1.4040878

24. Schmidt PA, Schmitz P, Zaeh MF (2016) Laser beam welding of electrical contacts for the application in stationary energy storage devices. J Laser Appl 28(2): 022423–1–6. https://doi.org/10.2351/1.4943908

25. Huang W, Wang H, Rinker T, Tan W (2020) Investigation of metal mixing in laser keyhole welding of dissimilar metals. Mater Des 195:109056-1–109114. https://doi.org/10.1016/j.matdes.2020.109056

26. Hummel M, Külkens M, Schöler C, Schulz W, Gillner A (2021) In situ X-ray tomography investigations on laser welding of copper with 515 and 1030 nm laser beam sources. J Manuf Processes 67:170–176. https://doi.org/10.1016/j.maapro.2021.04.063

27. Li Z, Yu G, He X, Li S, Li Z (2020) Fluid flow and solute dilution in laser linear butt joining of 304SS and Ni. Int J Heat Mass Transf 161:120233-1–120316. https://doi.org/10.1016/j.ijheatmasstransfer.2020.120233

28. Trvassoli S, Abbasi M, Tahavvori R (2016) Controlling of IMCs layers formation sequence, bond strength and electrical resistance in AlCu bimetal compound casting process. Mater Des 108:343–353. https://doi.org/10.1016/j.matdes.2016.06.076

29. Otten C, Reisgen U, Schmachtenberg M (2016) Electron beam welding of aluminum to copper: mechanical properties and their relation to microstructure. Weld World 60:21–31. https://doi.org/10.1007/s40194-015-0280-x

30. Yan S, Shi Y (2019) Influence of laser power on microstructure and mechanical property of laser-welded Al/Cu dissimilar lap joints. J Manuf Process 45:312–321. https://doi.org/10.1016/j.jmapro.2019.07.009